Impact of three different TiO2 morphologies on hydrogen evolution by methanol assisted water splitting: Nanoparticles, nanotubes and aerogels

Daniela d'Elia, Christian Beauger, Jean-François Hochepied, Arnaud Rigacci, Marie-Hélène Berger, Nicolas Keller, Valérie Keller, Yoshikazu Suzuki, J Valmalette, Mourad Benabdesselam, et al.

Impact of three different TiO_2 morphologies on hydrogen evolution by methonal assisted water-splitting: nanoparticles, nanotubes and aerogels.

(published in International Journal of Hydrogen Energy 36, 22 (2011) 14360-14373)

Daniela D'Elia [a, b, 1], Christian Beauger [a,], Jean-François Hochepied [b], Arnaud Rigacci [a], Marie-Hélène Berger [c], Nicolas Keller [d], Valérie Keller-Spitzer [d], Yoshikazu Suzuki [e, a], Jean-Christophe Valmalette [f], Mourad Benabdesselam [g], Patrick. Achard [a]*

(a) ***MINES ParisTech****, CEP/EM&P, Center for Energy and Processes, BP207, 06904 Sophia Antipolis Cedex, France*

(b) ***MINES ParisTech****, CEP/SCPI , Center for Energy and Processes,60 bd St Michel, 75272 Paris Cedex 06, France*

(c) ***MINES ParisTech****, Centre des Matériaux, CNRS UMR 763, BP 87, 91003 Evry Cedex, France*

(d) ***Laboratoire des Matériaux, Surfaces et Procédés pour la Catalyse****, CNRS UMR 7515, University of Strasbourg, 25 rue Becquerel 67087 Strasbourg, France*

(e) ***Graduate School of Pure and Applied Sciences****, University of Tsukuba, Ibaraki 305-8573, Japan*

(f) ***Institut Matériaux Microélectronique Nanosciences de Provence****, CNRS UMR 6242, Université du Sud Toulon Var, BP 20132, La Garde Cedex, 83957 Toulon, France*

(g) ***University of Nice Sophia-Antipolis,*** *Laboratory of Condensed Matter Physics, CNRS UMR 6622, Parc Valrose 06108 Nice cedex 2, France*

Abstract

Increasing the activity of a photocatalyst goes through the improvement of both its absorption (light) and adsorption (reactant) properties. For a given semiconducting material, the charge carrier separation is also a very important step. Properly combining chosen phases is one option to improve this separation (example of the commercial P25) and depositing platinum on the surface of the catalyst, another one. In some cases, coupling both may nevertheless lead to a decrease of photoactivity or at least limit the potentiality of the catalyst. A third option, consisting in modifying the morphology of the photoactive phase, has shown very promising results.

In this study, we have elaborated, characterized and evaluated the hydrogen evolution potentiality (through methanol assisted water splitting) of different TiO_2 morphologies : nanoparticles, nanotubes and aerogels. These materials have shown different behaviours depending on both their composition and morphology. Different types of separation processes have been claimed to account for the observed different photoactivities, with more or less pronounced synergetic effects, due to : the use of Pt as a co-catalyst, the mixture of different TiO_2 phases (anatase and TiO_2(B) or rutile) and the specific morphology of the samples (nanotubes or aerogels). Among all the tested samples, the TiO_2 aerogel supported Pt one exhibited very promising performances, three times as active as P25 supported Pt, which is already much more active than pure P25 in our testing conditions.

Keywords: TiO_2; photocatalysis; water splitting; morphologies; nanotubes; aerogels; hydrogen

* Corresponding author. *Tel.: +33 4 93 95 75 67; Fax.: +33 4 93 95 75 35;*
Email address: christian.beauger@mines-paristech.fr
[1] Present address : CAT Catalytic Center, ITMC, RWTH Aachen University, Worringerweg 1, D-52074 Aachen, Germany

1. Introduction

The energetic challenge of our century is to provide enough energy to a growing population with a minor impact on the environment. In the general context of the forthcoming energy demand increase, energy resources shortage and global warming, hydrogen may be a significant part of the future energetic landscape. Indeed, this need for new energy resources, non generating greenhouse gases, could be partially fulfilled with hydrogen, provided that the production processes are environmentally friendly.

The concept of direct solar energy conversion through water splitting (water photoelectrolysis) has already been validated on numerous semiconducting materials [1-4]. A lot of work has already been done on titanium dioxide (TiO_2) [5], beginning with the pioneer results obtained by Fujishima and Honda [6]. Both the optoelectronic properties and the chemical characteristics of the materials tested so far, as mediator in the $h\nu$ / H_2 conversion process, did not allow to find a satisfactory solution to obtain, under natural irradiation (sun), both a high conversion efficiency and a satisfactory material lifetime. In general, in the standard utilization conditions, an improvement of efficiency is concomitant with a diminution of the material stability. It is notably the case when titanium dioxide is replaced with sulphur-based compounds such as cadmium sulfide (CdS).

We believe that there is still room to improve the TiO_2 activity, especially by playing on its morphology [7]. As an example, the morphology of nanoparticles has a direct influence on the photo-activity by affecting the specific surface area, the hydrophilic character or the availability of charge carrier by modifying the internal electric field close to the surface (space charge effects). Moreover, a great anisotropy of particles induces distinct behaviors by giving more importance to some crystalline planes in contact with the surrounding environment. It should then be possible, if the grain growth can be controlled, to develop the crystalline faces corresponding to the higher photocatalytic activity.

The purpose of the work presented here is to check the influence of the morphology of different nanostructured TiO_2 samples. Three different types of material have been synthesized, following different routes, in the scope to obtain a representative panel of samples with various morphologies: individual nanoparticles, nanotubes and aerogels. Among the structurally and morphologically characterized samples, the most promising ones have been tested for water splitting, with methanol as a hole scavenger. Within this study, we have confirmed some common sense assumptions and demonstrated the soundness of utilizing aerogels as photocatalysts for the foreseen application. They revealed to be more active than Degussa P25, whatever the selected operating conditions. Some hypotheses have been proposed to discuss such an encouraging result.

2. Experimental

2.1 Materials

Two batches of individual nanoparticles, three of nanotubes and four of aerogels have been prepared and characterized for this study. The selected samples have then been tested and their performances compared with those of commercial samples, namely Degussa P25 and Alfa Aesar anatase (*ref. 036199*).

2.2 Elaboration

2.2.1 Nanoparticles

TiO_2 nanoparticles have been synthesized by precipitation of titanium chloride ($TiCl_4$, *Fluka 89545*) in aqueous sodium hydroxide solution (NaOH, *Sigma Aldrich S8045*) followed by crystallisation in autoclave (hydrothermal transformation):

- a 250 ml $TiCl_4$ solution (0.4 M in water, containing 10 ml of HCl) and a 250 ml NaOH solution (2 M) are simultaneously added to 500 ml of distilled water, under mechanical stirring for one hour, at atmospheric pressure, maintaining the pH at 2 with 1.6 M NaOH and the temperature at 25 °C;
- the obtained amorphous precipitate is then washed three times with distilled water and added to distilled water to prepare a suspension at pH = 10 (adjusted with 1.6M NaOH);
- finally, the crystallisation is performed with 150 ml of the prepared suspensions introduced in a 300 ml Teflon lined Hastelloy autoclave, heated at 150 °C or 250 °C for 18 h under gentle magnetic stirring.

Starting from the native as-precipitated nanoparticles, two types of samples have thus been prepared depending on the temperature of the hydrothermal treatment: NP150 [pH = 10; T = 150 °C] and NP250 [pH = 10; T = 250 °C].

2.2.2 Nanotubes

Nanotubes have been prepared following the hydrothermal transformation route developed by Kasuga [8] and already used in a former study [9]:

- 8 g of commercial TiO_2 anatase (*99.9% Alfa Aesar 036199*) added to 100 ml of 10M NaOH (*Sigma Aldrich S8045*) are introduced in a 300 ml Teflon lined Hastelloy autoclave, heated at 150 °C for 72 hours under stirring;
- the sodium titanates thus obtained are then washed at room temperature, three times with distilled water;
- hydrogen titanates are obtained by ion exchange, realized three times with 2 M hydrochloric acid (HCl *Fluka 84415*) : adjustment of the final suspension pH to 2, stirring 4 h at room temperature, centrifugation and washing three times with distilled water at room temperature;
- hydrogen titanates are then dried and calcined in static air for 2 h at 400, 500 and 600 °C (2 °C/min).

Three types of samples have thus been prepared: NT400, NT500 and NT600.

2.2.3 Aerogels

Aerogels have been prepared following an acid-catalysed sol-gel route followed by a drying process under supercritical conditions [10] and a calcinations step.

- 100 ml of sol are prepared by slowly adding an aqueous solution of nitric acid (2 M HNO_3, *Riedel-de Haën 35278*), partially diluted in isopropanol (iPrOH purum > 99.0%, *Fluka*

59310) (2.3 ml HNO_3, 0.9 ml H_2O, 58.2 ml iPrOH), to an alcoholic solution of titanium tert-butoxyde ($Ti(OC_4H_9)_4$, *Fluka 86910*) (19.2 ml $Ti(OC_4H_9)_4$, 19.4 ml iPrOH), under continuous mechanical stirring. These proportions correspond to the following molar ratio, defined by Boudjay et al. [11] in their early works : $Ti(OC_4H_9)_4$ / iPrOH / HNO_3 (2 M) / H_2O = 1 / 18 / 0.08 / 3;

- the gel, obtained after 30 min in room conditions, is covered with iPrOH and aged 4 days at room temperature before being thoroughly washed with iPrOH, in order to eliminate traces of water;
- aerogels are then obtained after supercritical (SC) drying with CO_2, in three steps : i) solvent exchange (iPrOH with SC CO_2 / 80 bars, 37 °C, 5 kg_{CO2}/h, 4 h), ii) isothermal depressurization to atmospheric pressure (0.05 bar/min, 37 °C) and iii) inertial cooling down to room temperature;
- finally, the so-called aerogels are milled in an agate mortar and calcined for 2 h in air between 400 and 700 °C (2 °C/min).

Two batches of five aerogel samples have thus been prepared: AG (not calcined), AG400, AG500, AG600 and AG700

2.2.4 Platinum deposition

Pt nanoparticles have been synthesized at the surface of the materials by classical wet impregnation of TiO_2 under magnetic stirring at room temperature with an hexachloroplatinic acidic aqueous solution (H_2PtCl_6, x H_2O *Aldrich 254029, 99.995%*) so as to obtain a ratio Pt/TiO_2 = 0.3 wt% (5 ml water / g TiO_2). After evaporation of the solvent and drying at 110 °C for 1 h in air, the materials were calcined at 350 °C for 1 h in flowing air and finally reduced under flowing H_2 at 350 °C for 1 h to get metallic nanoparticles.

2.3 Characterizations

All the samples have been characterized so as to determine their structure, morphology and optical properties.

2.3.1 X-Ray Diffraction

The crystallographic structure has been determined by X-Ray Diffraction using a Bruker *D8* diffractometer [(θ -2θ mode, cobalt source (Co Kα = 1.79 A), counting time = 0.43 s, step = 0.0144°, range = 10-90°].

2.3.2 High Resolution Transmission Electron Microscopy

A Tecnai *F20 ST* HR-TEM with a point to point resolution of 0.24 nm has been used to observe the particles: shape, size and local crystallographic structure from the lattice planes, matrix defects. The samples are deposited on *Agar Scientific* analysis grids: *Holey Carbon Film 300 Mesh Cu* for nanoparticles and *Formvar/Carbon 300 Mesh Cu* for nanotubes.

2.3.3 Nitrogen Sorption Analysis

The specific surface area has been determined based on the BET model, using a Micromeritics *ASAP 2010* to collect the N_2 sorption isotherms. The samples are first outgassed overnight at 60 °C under vacuum, before being analysed, at 77 K.

2.3.4 Diffuse Reflectance UV-Vis Spectroscopy

In order to determine the light absorption range of powder samples, Diffuse Reflectance spectroscopy has been used in the UV-Visible region, with the help of an integration sphere. These measurements have been carried out on a CARY 500 UV-VIS-NIR spectrophotometer, between 300 and 600 nm.
Black paper and Teflon powder have been used as references respectively for 0% and 100% reflectance. The results have essentially been used to determine the band gap of the analysed materials as follows [12, 13].

Making the assumption that the Kubelka-Munk function F(R) is proportional to the absorption coefficient, we have:

- $[F(R).\ h\nu]^{0.5} \ \alpha \ (h\nu - Eg)$ for an indirect band gap
- $[F(R).\ h\nu]^{2} \ \alpha \ (h\nu - Eg)$ for a direct band gap

where h is the Planck's constant, ν the frequency (s^{-1}) and Eg the band gap energy value (eV).

If the absorption edge gives a rough estimation of the band gap, plotting $(F(R)h\nu)^n$ as a function of hν, allows to more precisely determine the value of the band gap that is equal the x-intercept of the extrapolated linear part of the plot.

2.3.5 Raman spectroscopy

Measurements have been carried out on a LabRAM HR Raman spectrometer using 514.5 nm excitation wavelength, an objective 100X and a 1800 line mm^{-1} grating. The resulting power on the sample is about 2 mW on a diffraction limited area about $1\mu m^2$. This characterization technique has been used to quantify the respective amounts of anatase and $TiO_2(B)$ in some of our samples, following the method proposed by Beuvier et al. [14]. I_A, the area of the main peak of anatase (144 cm^{-1}), and I_B, that of the main peak of $TiO_2(B)$ (123 cm^{-1}), are proportional to m_A and m_B , respective weights of anatase and $TiO_2(B)$ in the sample: $I_A = m_A.\sigma_A$ and $I_B = m_B .\sigma_B$, where σ is the scattering factor of the corresponding peak. Drawing $x_A = m_A/(m_A + m_B)$ as a function of $y = I_A/(I_A + I_B)$, for several mixtures of known composition, allowed Beuvier et al. to set-up the following formula: $x_A = y / [k_R + (1 - k_R).y]$ where k_R, the anatase Raman sensibility factor ($k_R = \sigma_A / \sigma_B$), equals 6.2.

2.4 Photocatalytic activity

Once characterized, the materials have been tested for hydrogen evolution with or without Pt deposit.
Two cylindrical photolysis reactors (one in Strasbourg-France [15] and one in Kyoto-Japan [16]) have been used, in the center of which is placed an irradiation source, water cooled thanks to a surrounding double walled quartz jacket.

A 1 litre suspension of the catalyst is prepared with deionized water and MeOH (10 vol%) as a sacrificial agent (to favour the hydrogen evolution [17, 18]) and irradiated under magnetic stirring. Before irradiation, the suspension is outgassed under inert gas bubbling, for 90 min, in order to evacuate the oxygen from both the suspension and the free space of the reactor.

The hydrogen evolved under irradiation is analyzed by a micro-Gas Phase Chromatograph, calibrated with different H_2/N_2 standards.

The use of the two reactors mentioned above is justified by their peculiar specificities.

In the Laboratoire des Matériaux, Surfaces et Procédés pour la Catalyse (LMSPC, Strasbourg):

- the irradiation source is a 150 W metal halide lamp (*BLV-Licht, C-HIT, 150 W*) whose spectrum is more or less centered on the visible region (figure 1a);
- the hydrogen analysis is made under continuous nitrogen flow so that a hydrogen flow rate is actually measured.

In the Institute of Advanced Energy (IAE, Kyoto University):

- the irradiation source is a 450 W mercury vapour lamp (*Ushio, UM-452, 450 W*), more intense in the UV region than the metal halide lamp used in the previous reactor (figure 1b);
- the argon bubbling is stopped once the suspension has been outgassed, so the hydrogen evolved is accumulating in the free space of the reactor. Hence, here it is the total amount of hydrogen which is measured at the time of analysis.

The main difference stands in the type of lamp used, which will allow us to check the activity of our materials in different irradiation conditions (more or less energetic and powerful).

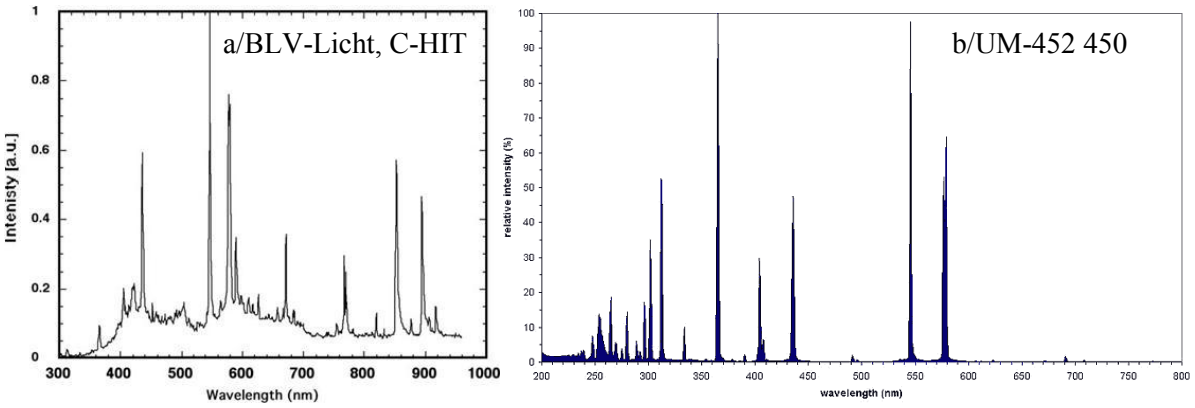

Fig. 1. Irradiation spectrum of the sources used at a) the LMSPC, Strasbourg, France () and b) the Institute of Advanced Energy, Kyoto, Japan (UM-452 450 W)

3. Results and discussion

3.1 Characterizations

3.1.1 Nanoparticles (NP)

The main structural and morphological features of the NP particles are reported in table 1.

Table 1. Structural and morphological features of commercial Degussa P25 and Alfa Aesar anatase, nanoparticles (NP), nanotubes (NT) and aerogels (AG) samples.

Sample	Calcination Temperature (°C)	Crystalline structure	Particle size* (nm)	Specific Surface Area S_{BET} (m^2/g)
Degussa P25	-	A/R 80/20 (wt%)	30	46
Alfa Aesar Anatase (*ref. 036199)*	-	A	180	7.4
NP150	150	A	10	143
NP250	250	A	90	17
NT300	300	B	-	246
NT400	400	A/B 80/20 (wt%**)	-	117
NT500	500	A / traces of B	-	90
AG	As-prepared	amorphous	-	569 (a) – 600 (b)
AG400	400	A	10	159 (a) – 150 (b)
AG500	500	A	15	95 (a) – 85 (b)
AG600	600	A/R	10/20	59 (a) – 60 (b)
AG700	700	R	200	6 (a)

A = anatase, R = rutile, B = TiO_2(B)
a = batch # 1, b = batch # 2
** from TEM observations*
*** determined by Raman spectroscopy*

All the prepared samples are composed of anatase TiO_2 (figure 2). As expected, the higher the autoclave treatment temperature, the better the crystallinity, the bigger the particles and the lower the specific surface area.

So considering the foreseen application, we will focus on the low temperature treated nanoparticles NP150 (figure 3), which is composed of the smallest pure anatase nanoparticles responsible of a reasonable specific surface area (143 m^2/g). This sample has then been optically characterized.

The band gap of NP150 has not surprisingly been estimated to 3.2 eV after reflectance data treatment, assuming an indirect band gap [19-22] (figure 4a). The assumption of a direct band gap, reported by some authors for nanoparticles [23] or crystals [24], would give, with this determination protocol on our materials, a value of 3.45 eV which is inconsistent with literature data reported for anatase particles [25, 26]. Such a large value could have been considered, due to the very small size of the particles. However, the assumption of an indirect bandgap is confirmed by the determination of that of NP250 (figure 4b), made up of larger particles (3.2 eV for an indirect bandgap also). Tolbert et al reported that the quantum behaviour does not depend on the nature of the bandgap (direct or indirect)

[27]. Moreover, according to Monticone et al. [22], it seems that the quantum size effect is rather limited on anatase, due to a very small exciton Bohr radius. No increase of the bandgap has been observed before diameter lower than 1.5 nm. Finally, Nozik et al. reported 3.45 eV and 3.59 eV as values for the first allowed direct transition (respectively corresponding to perpendicular and parallel light transitions) [28].

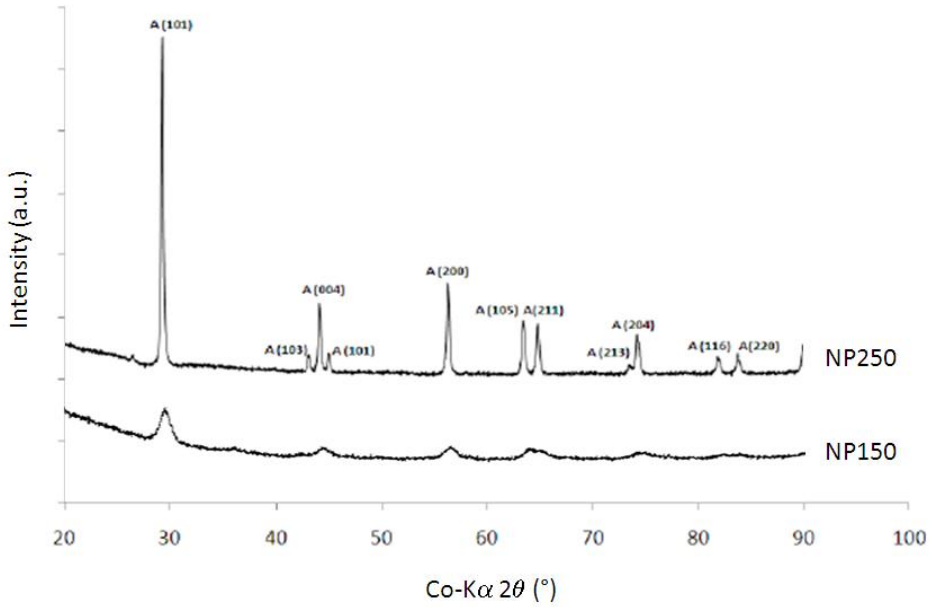

Fig. 2. XRD pattern of the nanoparticles NP150 and NP250, calcined at T = 150 °C and 250 °C respectively, from the alkaline suspension (pH=10)

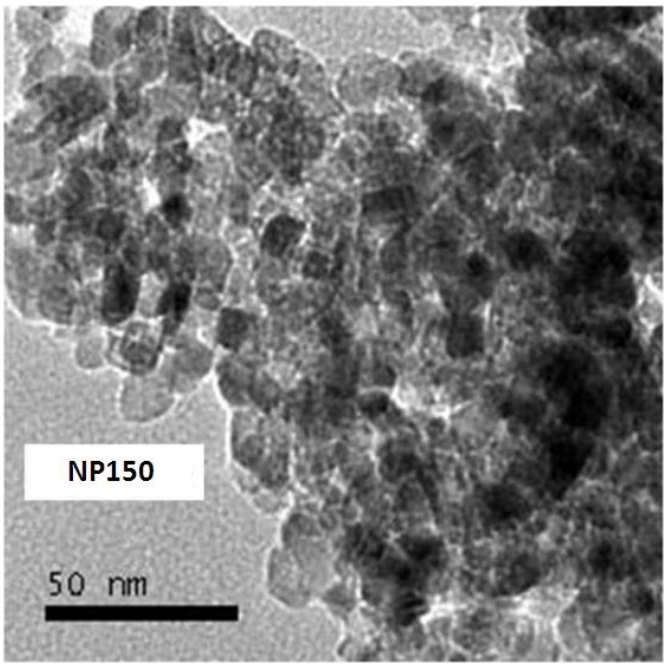

Fig. 3. TEM picture of the nanoparticles NP 150, calcined at T = 150 °C, from the alkaline suspension (pH=10).

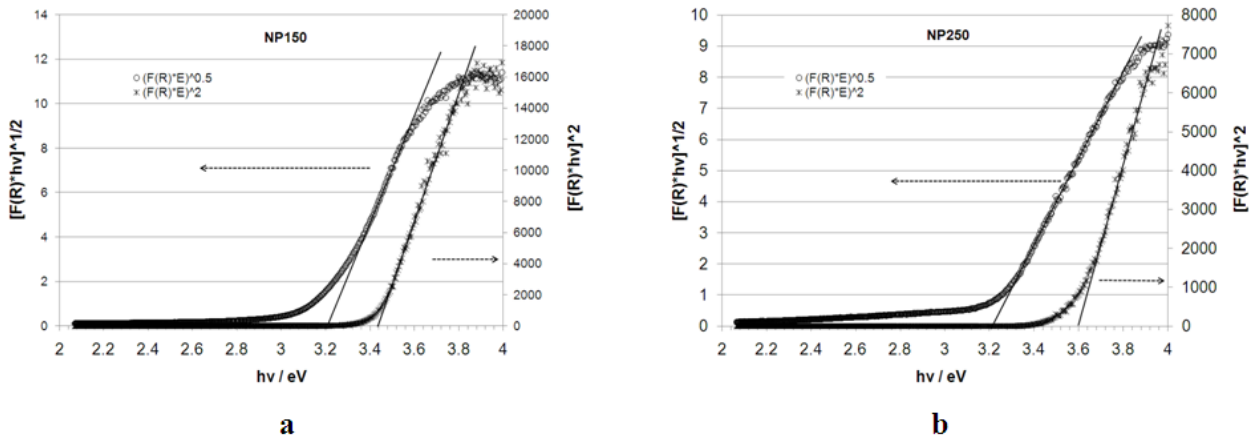

Fig. 4. Band gap estimation of the nanoparticles : a) NP150 (calcined at T = 150 °C) and b) NP250, (calcined at T = 250 °C)

3.1.2 Nanotubes (NT)

The main structural and morphological features of the NT samples are reported in table 1. Figure 5 shows the XRD patterns of the NT samples for different calcination temperatures.

The TiO_2(B) phase appears as the only detected one after calcinations at 300 °C as already reported in the literature [29]. Neither XRD nor HR-TEM allowed us to find any trace of anatase.

Anatase appears as the main phase after calcination at 400 °C (NT400). A significative amount of TiO_2(B) still remains in this sample. Raman spectroscopy (figure 6) allowed us to identify both anatase [30] and TiO_2(B) [31] characteristic vibration modes. After subtraction of the background and decomposition of the two TiO_2 contributions, the quantification method presented in 2.3.5 allowed us to estimate the amount of anatase in NT400 to 80 wt%, the remaining phase being TiO_2(B) (20 wt%).

Finally, both phases are still present after calcination at 500 °C, in NT500, which is particularly well crystallised. TiO_2(B), a very minor component in NT500, has been identified on TEM pictures (figure 7).

From a morphological point of view the samples are tube-like, with, at least for NT300 and NT400, typical length and diameter of 50-100 nm and 10 nm respectively (as evaluated from TEM observations). From 400 °C and above, they tend to decompose into nanoparticles after calcination. The higher the temperature of calcination, the lower the specific surface area and the more pronounced the degradation into nanoparticles (figure 8). Cross-checking TEM observations and XRD results, it seems highly probable that, in our samples, nanotubes are made of TiO_2(B) while only particles issued from their decomposition are made of anatase.

These samples have been optically characterized in order to determine their band gap value. It decreases with increasing calcination temperature, from 3.35 eV for NT300 (TiO_2(B)) down to 3.25 eV for NT500 (anatase).

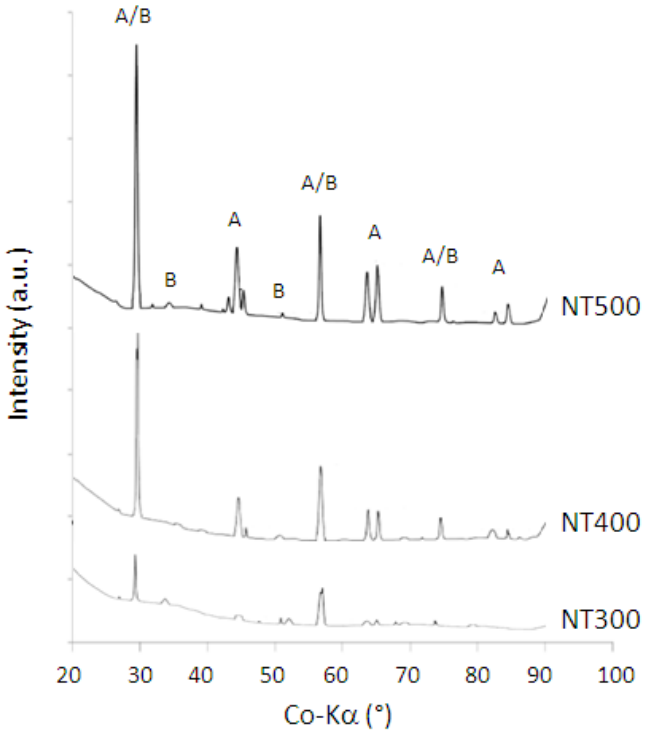

Fig. 5. XRD patterns of the nanotubes NT300, NT400 and NT500 (NT calcined at 300, 400 and 500 °C).

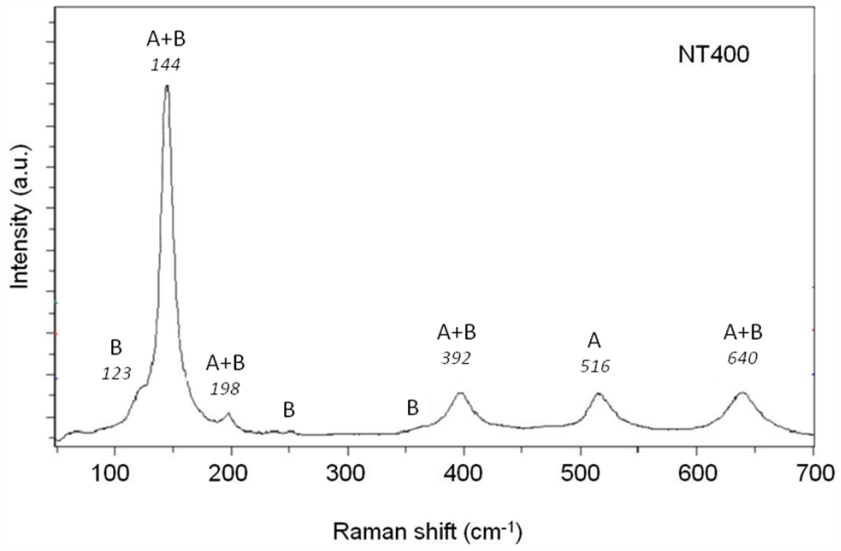

Fig. 6. Raman spectrum of the nanotubes NT400 (NT calcined at 400 °C), A=anatase, B=TiO_2(B).

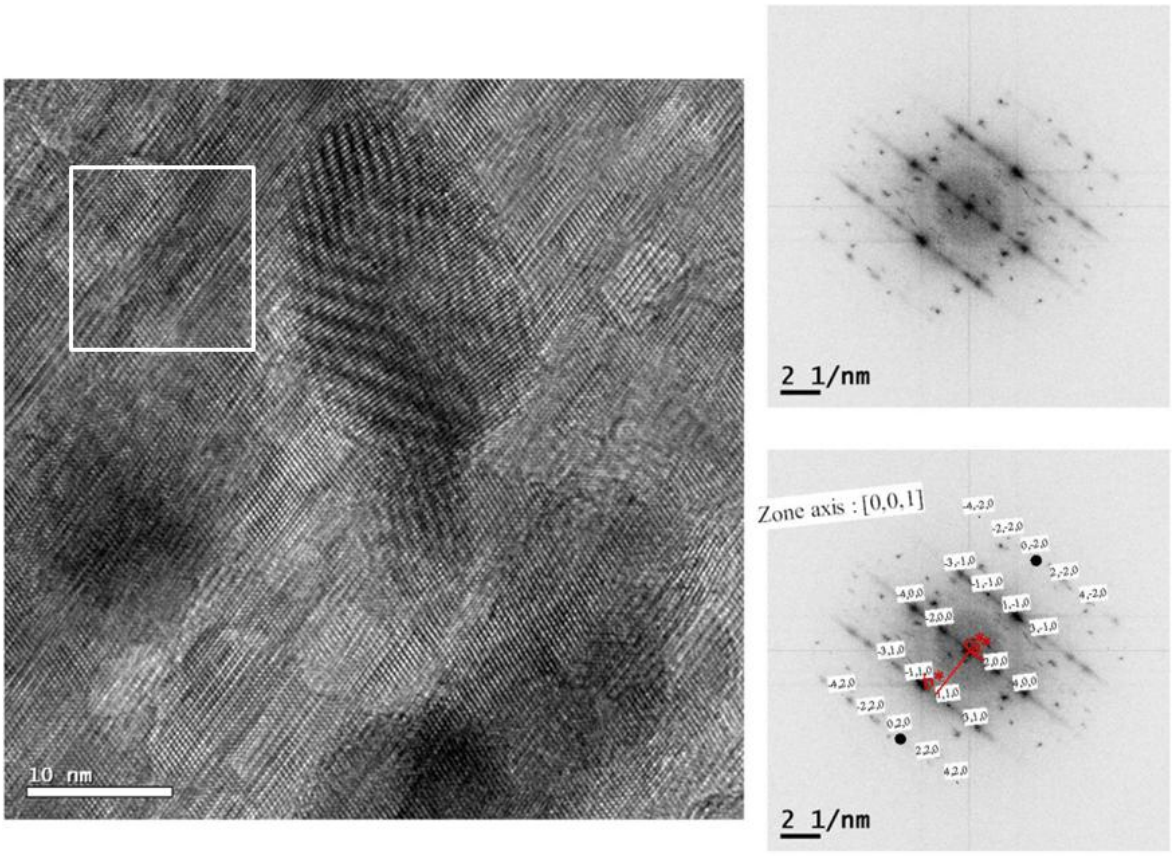

Fig. 7. TEM picture of the nanotubes NT500 (NT calcined at 500 °C) evidencing the presence TiO_2-B (FFT realized on the white square).

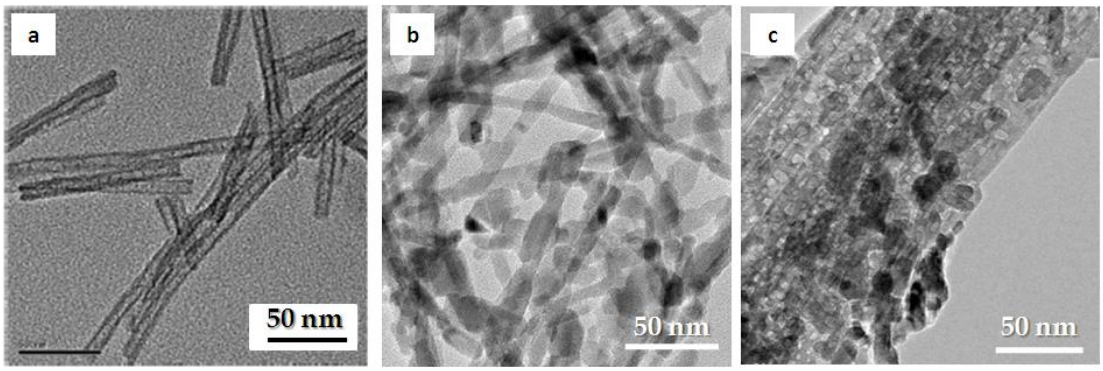

Fig. 8. Modification of the nanotubes morphology with the calcination temperature, a) NT300, b) NT400, c) NT500.

3.1.3 Aerogels (AG)

The main structural and morphological features of the aerogels samples (AG) are reported in table 1.

Calcined at 400 °C, the samples are made of anatase. The anatase-rutile phase transition has been observed for a calcination temperature between 500 and 600 °C (figure 9). At 700 °C, the only detected phase corresponds to rutile. The calcination temperature of our aerogel samples has thus been selected at 500 °C, in order to reach both a sufficient crystallinity and an acceptable specific surface area (97 m²/g) while avoiding the presence of rutile.

This sample (AG500), whose TEM picture is shown on figure 10, has then been optically characterized and its indirect bandgap value evaluated at 3.25 eV (the assumption of a direct bandgap would give a value of 3.6 eV).

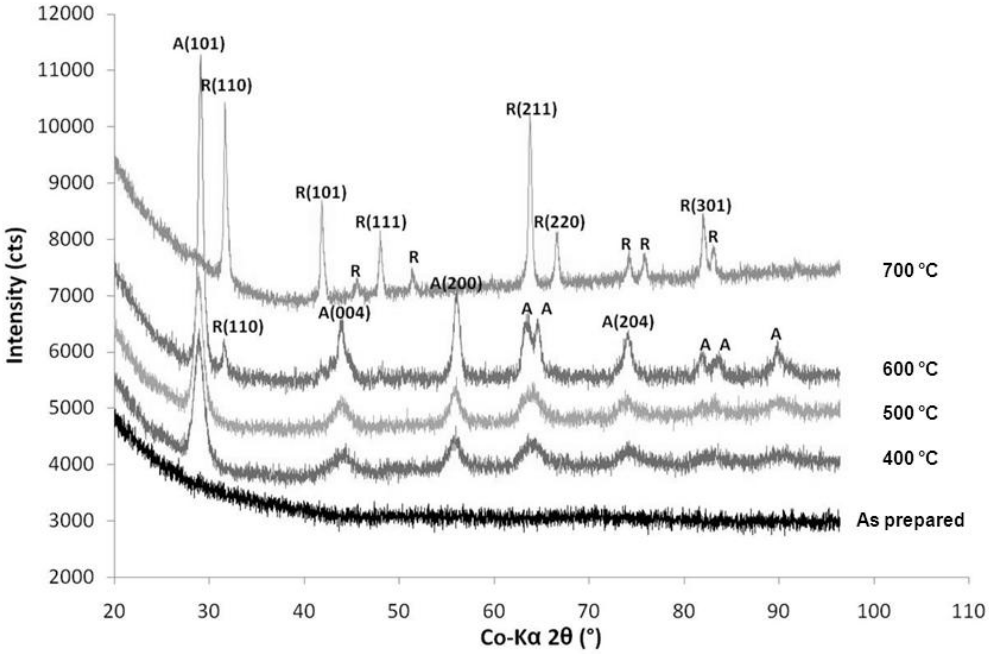

Fig.9. Evolution of the XRD pattern of TiO_2 aerogels with the calcination temperature.

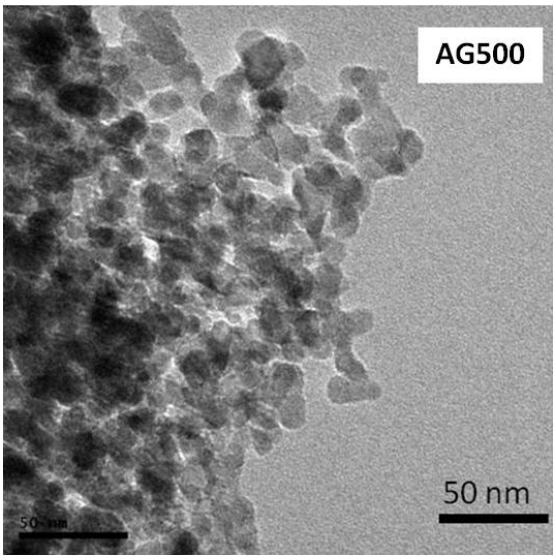

Fig. 10. TEM picture of TiO_2 aerogels calcined at 500 °C (AG500).

3.2 Photocatalytic activity

The different selected materials prepared within the framework of this study have been tested for H_2 evolution by methanol assisted water photolysis and their behavior compared to that of reference materials, namely commercial anatase TiO_2 from Alfa Aesar (*ref. 036199*) and P25 from Degussa.
The main structural and morphological features of the reference samples are also reported in table 1.

3.2.1 Nanoparticles (NP 10-150)

NP150 nanoparticles revealed a photocatalytic activity (0.31 µmolH_2/min) between that of the selected commercial anatase particles Alfa Aesar (0.1 µmolH_2/min) and Degussa P25 (0.37 µmolH_2/min), the latter exhibiting the highest activity (figure 11). This can be ascribed to both the composition (crystal phase) and the morphology of the samples.
On one hand, our nanoparticles, made of pure anatase, have a higher specific surface area than the selected commercial anatase ones, mainly due to smaller particles. The photocatalytic activity being strongly related to the available surface area in contact with water, the observed result is consistent with the fact that the higher the specific surface area, the higher the activity.
On the other hand, despite a lower specific surface area, the slightly better behavior of P25 may be due to its particular composition, a mixture of rutile and anatase TiO_2, favorable to an enhanced charge separation [32].
So the specific surface area, obviously being a major feature of photocatalysts, is probably not as important as the charge separation enhancement. These effects will be studied hereafter through the evaluation of TiO_2 nanotubes and aerogels that exhibit very particular morphological features, which should also act on the charge separation.

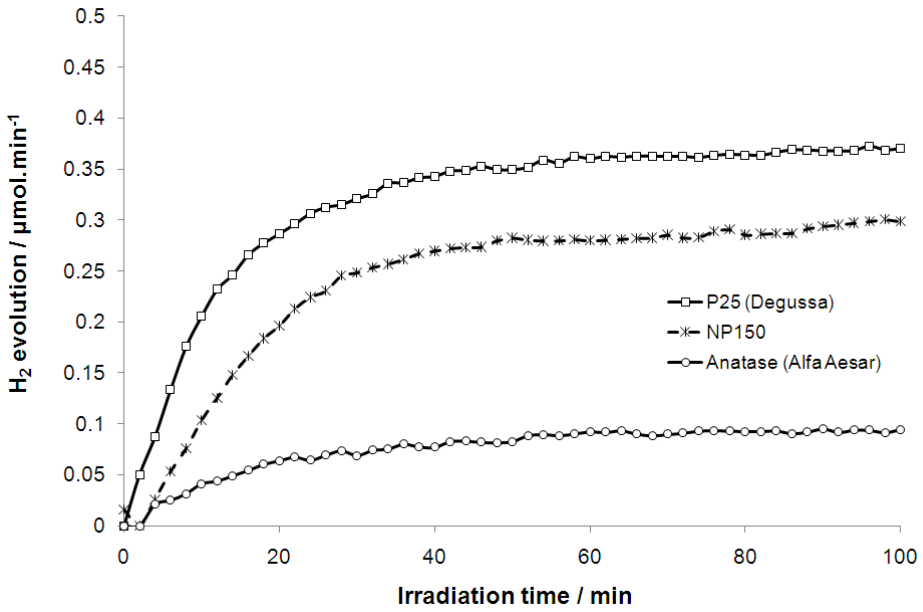

Fig. 11. H_2 evolution on TiO_2 nanoparticles NP150 (pH = 10, $T_{calc.}$ = 150 °C) compared to P25 (Degussa) and anatase nanoparticles (Alfa Aesar) - 150 W metal halide lamp, 0.9 l water + 0.1 l MeOH, 0.7 g samples, room temperature – Strasbourg, France.

3.2.2 *Nanotubes (NT)*

The different nanotube samples show diverse behaviors depending on their calcination temperature (figure 12).

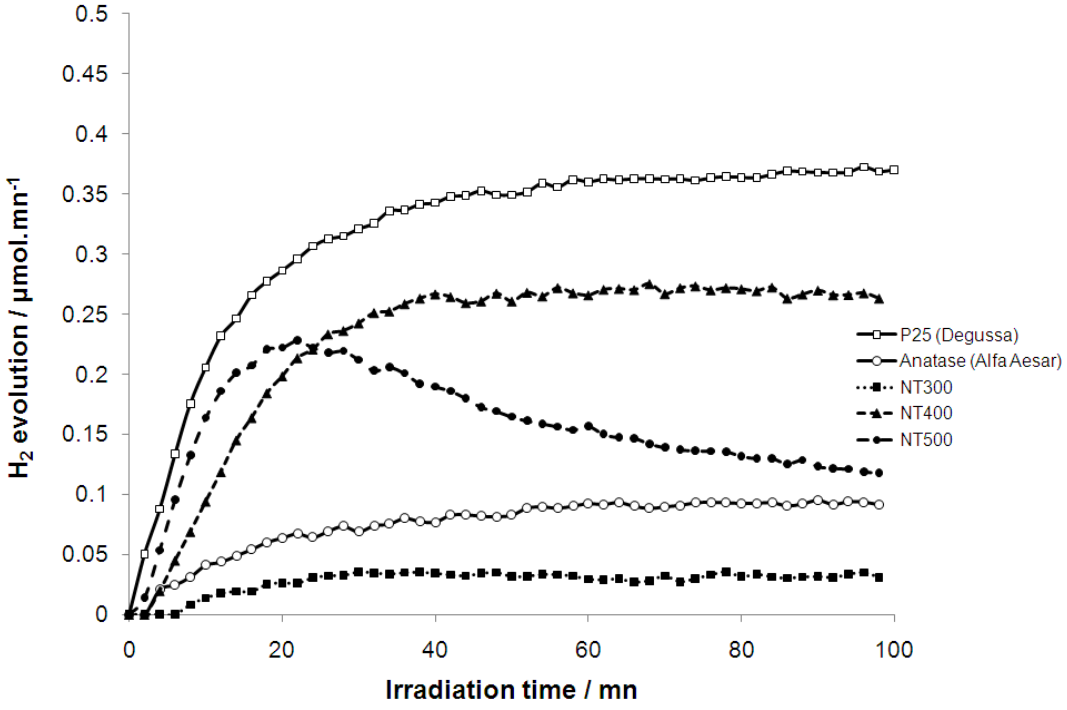

Fig. 12. H_2 evolution on TiO_2 nanotubes compared to P25 (Degussa) and anatase nanoparticles (Alfa Aesar) -150 W metal halide lamp, 0.9 l water + 0.1 l MeOH, 0.7 g samples, room temperature – Strasbourg, France.

First of all, NT300, calcined at 300 °C, is the less active of the tested materials, even if it has the highest specific surface area. It is actually composed of TiO_2(B), whose activity has already been observed to be lower than that of anatase [33-35]. Moreover a 3.35 eV bandgap has been measured, slightly higher than that of anatase, what can partially account for the lower photocatalytic activity in the testing conditions.

The two others, NT400 and NT500, are more active than the selected commercial anatase particles. They are mainly composed of anatase (80 wt% for NT400 and almost 100 wt% for NT500), accounting for their measured bandgap, close to 3.25 eV.

The higher the calcination temperature, the lower the amount of TiO_2(B) and the better the cristallinity (as evidenced by Raman spectroscopy and XRD results). Both evolutions are consistent with the observed photocatalytic activities. NT400 (0.27 µmolH_2/min) is indeed much more active than NT300 (0.04 µmolH_2/min). As regards NT500, it is notably more active than NT400 during the first 15 min of the experiment, before its activity begins to decline, to end around that of the selected commercial anatase particles. TEM observations gave evidence that the higher the calcination temperature the less stable the nanotubes. They actually tend to decompose into nanoparticles. A TEM observation of NT500 after test (figure 13), seems to reveal a more pronounced decomposition than before test. The observed behavior is thus not that surprising, and may partially be ascribed to the loss of the particular

1D morphology or the weakest interaction of the nanoparticles with the remaining TiO_2(B) nanotubes. Finally all the samples are less active than P25. Neither their specific surface area, nor the tubular morphology of the remaining TiO_2(B), was it assumed to improve the charge separation thanks to an increased conductivity along the tube axis, seems to be a strong enough lever to drastically improve their performances in comparison with P25, at least in the operated testing conditions. The crystallographic phases in presence have here to be discussed. The comparison between P25 (80 wt% A, 20 wt% R) and NT400 (80 wt% A, 20 wt% TiO_2(B)) is particularly interesting since they are both made up of two phases, with one in common and in similar proportion: anatase. In the considered irradiation conditions, we can expect the following order of light absorption efficiency : rutile (3 eV) > anatase (3.25 eV) > TiO_2(B) (3.35 eV), which may partly explain the better activity of P25 (A+R) compared to that of NT400 (A+B). Moreover, the charge separation process due to the contact between the two TiO_2 phases seems to be more efficient with P25 than with NT400, which actually has not been specifically designed for such a purpose. Considering the composition of NT400 and P25, the respective positions of the conduction bands of rutile, anatase and TiO_2(B) may also partly account for the better activity of P25 in the considered irradiation conditions.

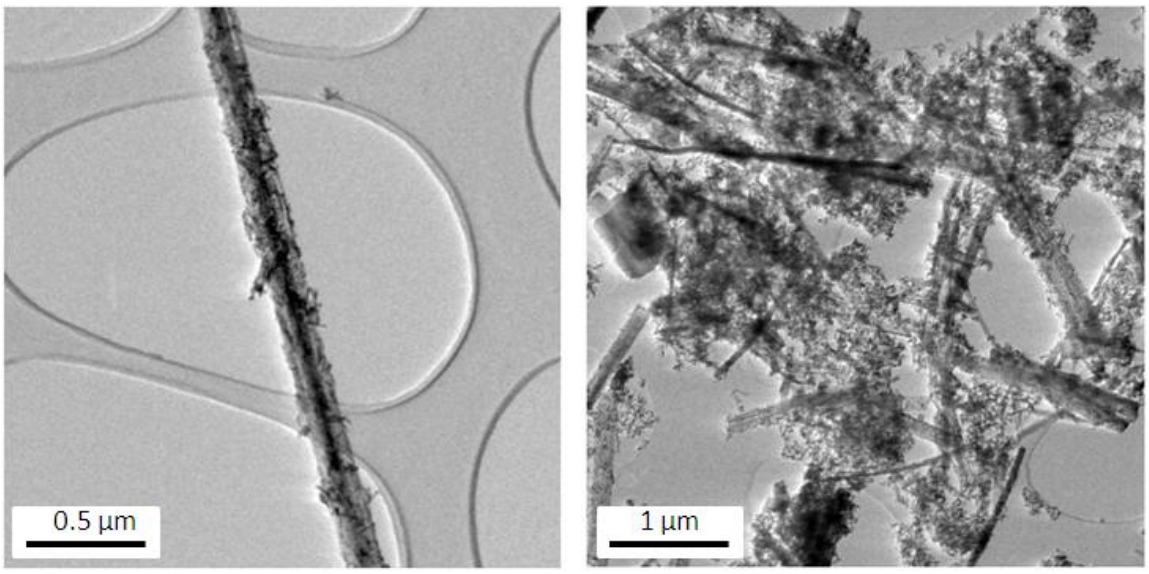

Fig. 13. TEM picture of NT500 (NT calcined at 500 °C) before (left) and after (right) H_2 evolution test.

It is noteworthy that when irradiated with a mercury vapor lamp, instead of a metal halide one, NT400 revealed to be more active than P25 (figure 14). In such conditions, the incident photons are more energetic and NT400 is more efficient, probably due to the higher activity of the TiO_2(B) part, leading to an enhanced charge separation (compared to former irradiation conditions). Compared to P25, this charge separation process may not anymore be as a determining step. Another process, related to the charge conductivity along the tube axis may be evoked to account for an additional charge separation effect and hence an increased activity of NT400 compared to P25, in such irradiation conditions.

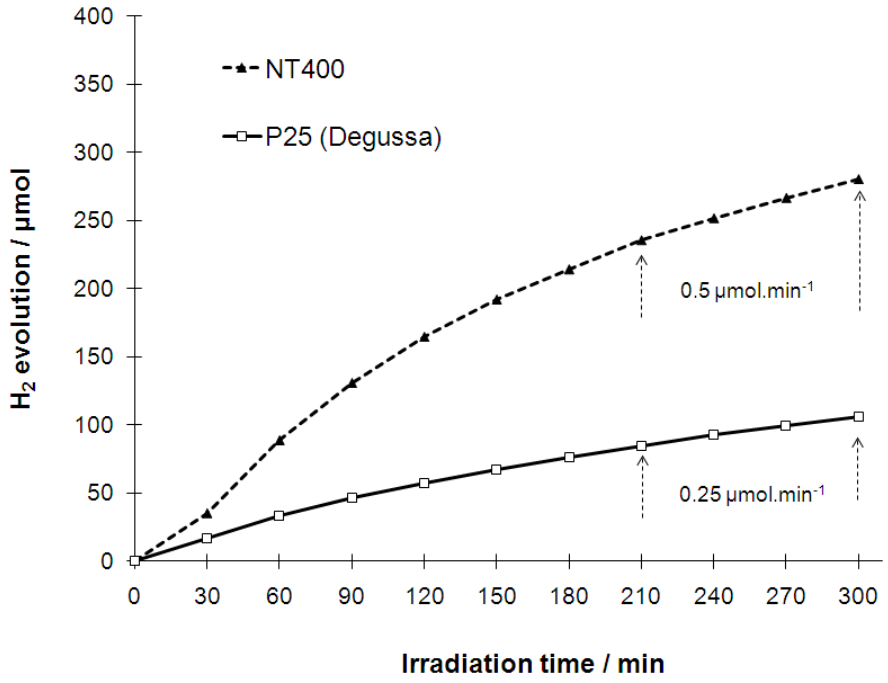

Fig. 14. H_2 evolution on TiO_2 nanotubes calcined at 400 °C compared to P25 (Degussa) - 450 W Hg lamp, 0.72 l water + 0.08 l MeOH, 0.8 g samples, 30 °C – Kyoto, Japan.

3.2.3 Aerogels (AG)

The sample referenced AG500 has been selected based on structural and morphological characterization results. Compared to P25, a slightly better photocatalytic activity has been observed (figure 15): 16 % relative increase from 0.37 µmolH_2/min for P25 to 0.43 µmolH_2/min for AG500. This value has been confirmed in a complementary experiment carried out in the japanese photoreactor (figure 16).

At least, four parameters can be referred to, in order to explain such a behavior, i) the specific surface area, ii) the surface chemistry, iii) the connectivity of the particles and iv) the crystallinity.

AG500 unfolds a significantly higher specific surface area than P25 (97 m²/g versus 46 m²/g), what could account for part of its good activity, in correlation with better adsorption properties as already mentionned by Dagan and Tomkiewicz [36] for the photoassisted oxidation of salicylic acid for instance. However, as shown earlier, this is probably not a completely satisfaying justification. All the more so that this sample is composed only of anatase whereas P25 is a mixture of anatase and rutile TiO_2 and should see its activity enhanced compared to that of AG500, because of a better charge carrier separation.

The surface chemistry of the particles may also in this case play a significant role. As a matter of fact, aerogels are prepared following a wet chemistry route, involving water and alkoxides, all the process being realized at a relatively low temperature. Hence, we can expect a higher surface concentration of titanol groups (≡ Ti–OH) for AG500 than for P25, responsible for a supposed higher hydrophilicity [37]. Znaidi et al. reported that the number of hydroxyl groups on the surface of TiO_2 aerogels only

slightly decreases up to 500 °C, compared to the as-prepared amorphous material [38]. Since the water splitting activity is closely related to the water adsorption efficiency at the surface of the catalyst, such surface chemical states are beneficial to the process.

Finally, the higher activity of the aerogel sample may partially be explained by its very particular texture. Indeed, whereas P25 is made up of individual particles forming agglomerates through electrostatic forces (Van der Waals bonds), in aerogels materials, the particles are strongly linked through real covalent bonds. With a reduced number of interfaces, such a texture may induce a better conductivity, beneficial to the charge carrier separation, as what could be expected for nanotubes.

The enhanced electronic conductivity mentioned above, is also strongly related to the cristallinity of the material, which is improved at higher calcination temperature. The higher the calcination temperature of the aerogel samples, the lower their specific surface area but the higher their photocatalytic activity (figure 16). This is also, by the way, another illustration of the relative importance of the specific surface area. Note that the activity of the sample calcined at 500 °C is comparable to that obtained in the previous test.

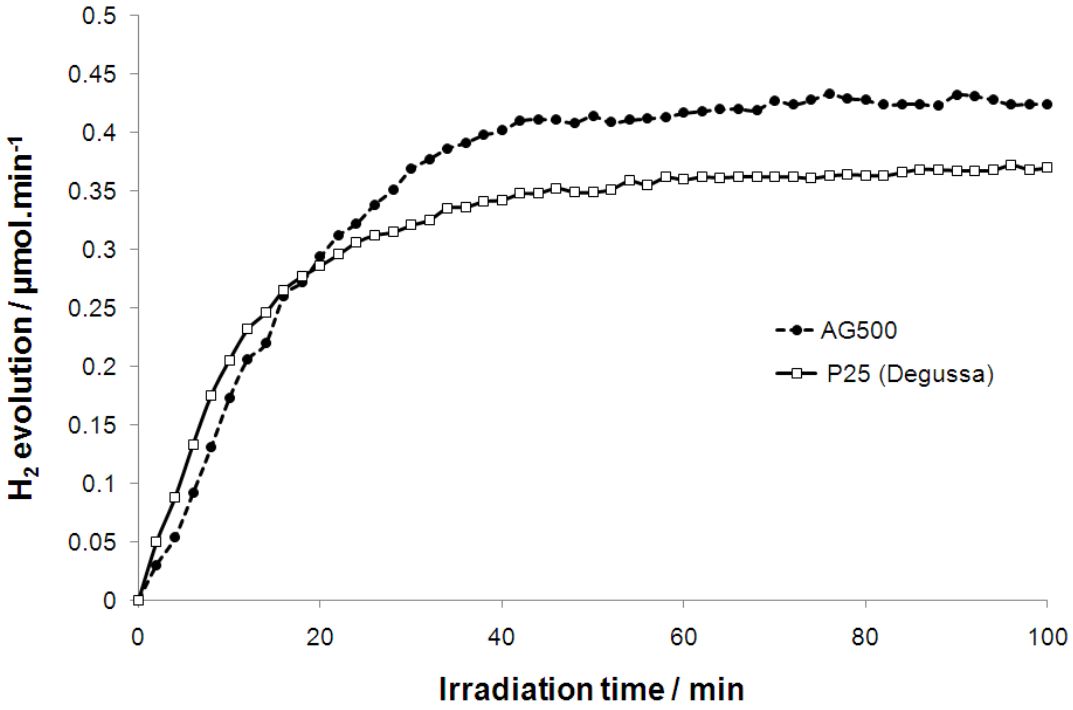

Fig. 15. H_2 evolution on TiO_2 aerogel calcined at 500 °C (AG500) compared to P25 (Degussa) - 150 W metal halide lamp, 0.9 l water + 0.1 l MeOH, 0.7 g samples, room temperature – Strasbourg, France.

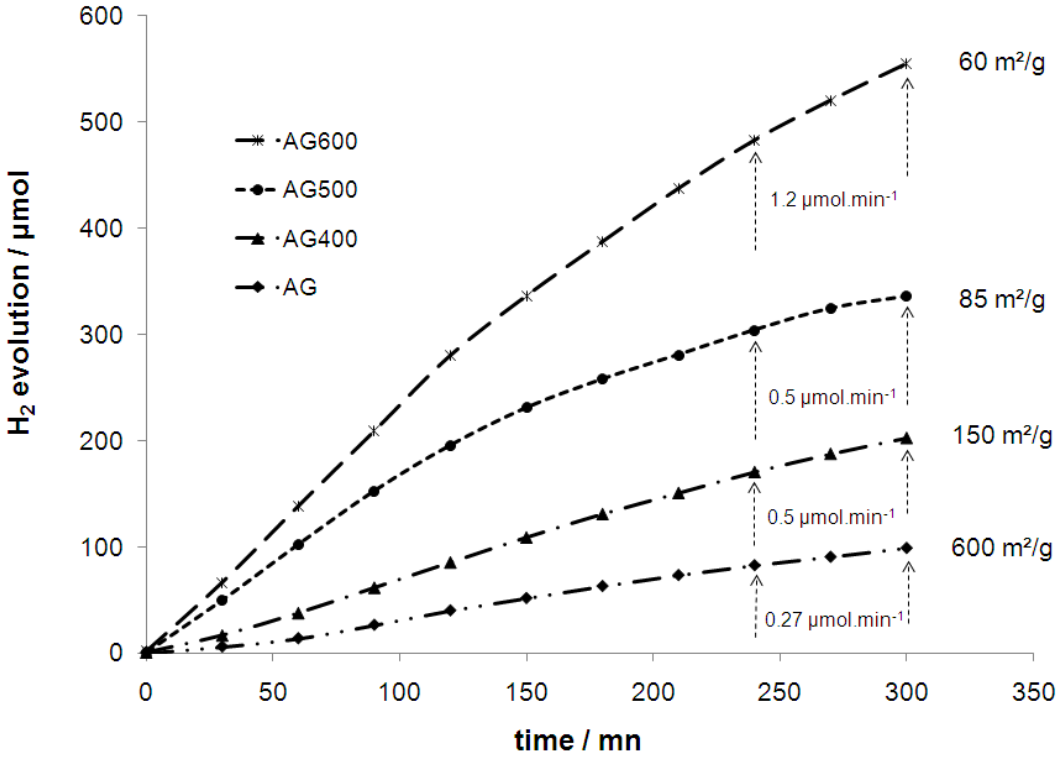

Fig. 16. H_2 evolution on TiO_2 aerogels calcined at different temperatures - 450 W Hg lamp, 0.9 l water + 0.1 l MeOH, 1 g samples, 30 °C – Kyoto, Japan.

Finally the promising AG500 sample has been loaded with platinum (0.3 wt%) in order to increase its activity [39-43]. STEM-High Angular Annular Dark Field (STEM-HAADF) microscopic observations evidenced that 2.5 nm Pt particles have been deposited on the surface of AG500 (figure 17), without any particular agglomeration. In comparison, TEM observation of Pt-P25 showed a similar Pt particles distribution on the surface, with a slightly lower average particle size (1.5 nm in diameter) (figure 18).

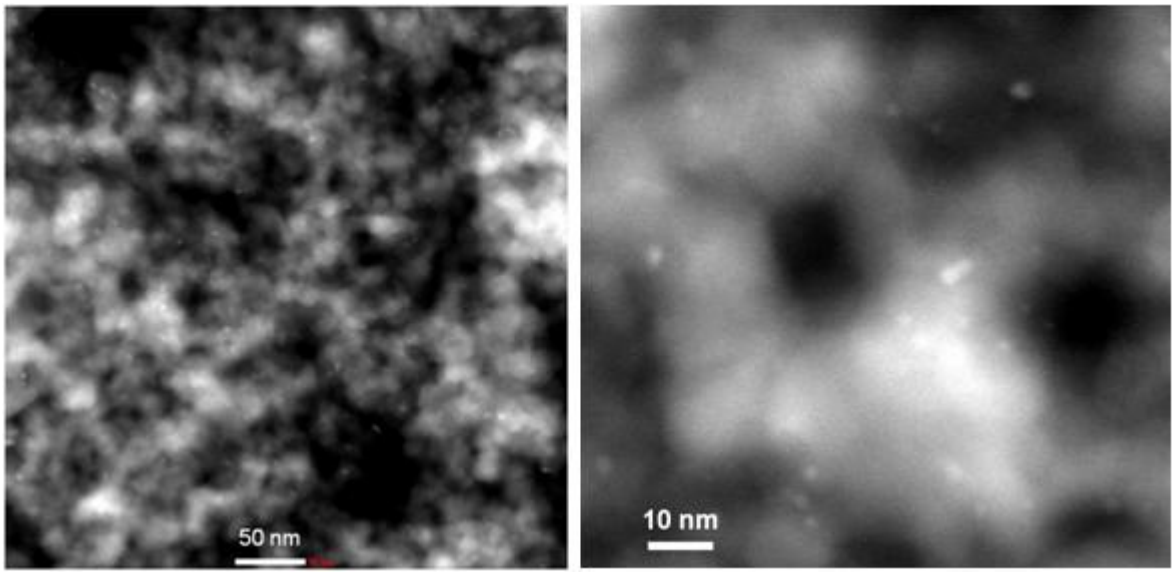

Fig. 17. STEM-HAADF pictures of AG500 supported Pt (0.3 wt%). White spots corresponds to Pt particles.

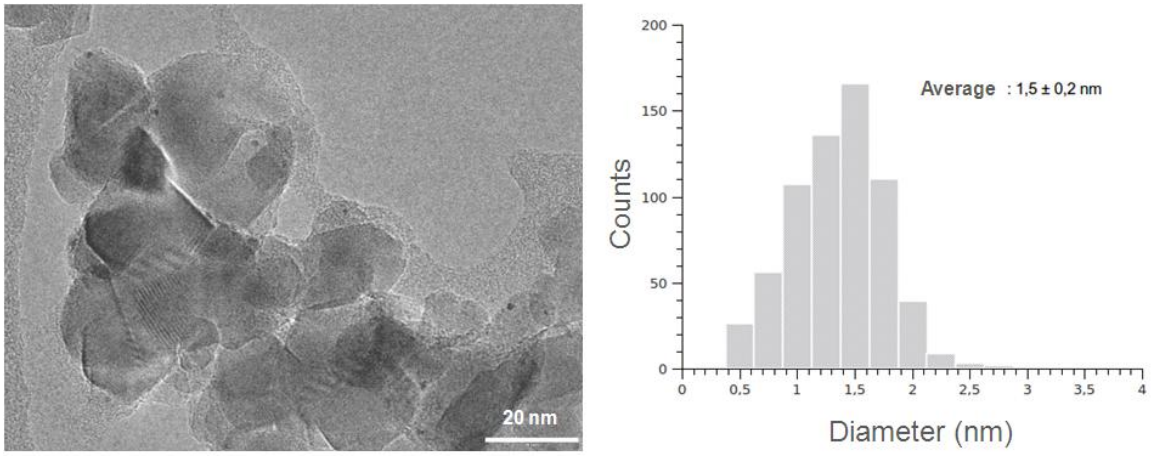

Fig. 18. TEM-HAADF picture of P25 supported Pt (0.3 wt%) (Black spots corresponds to Pt particles) and Pt particles size distribution (statistics on 656 particles).

Both Pt loaded samples (Pt-AG500 and Pt-P25) are much more active than bare TiO_2 photocatalysts, what can be ascribed to the beneficial effect of Pt nanoparticles in the charge carrier separation process [44]. Pt particles act as electron sinks one hand and, more important, catalyze the (dark) reduction of protons one the other hand. If this effect has already been well reported in the literature, more surprising is the behavior of the aerogel supported Pt sample. It remains more active than Pt-P25 but the difference of performance is significantly increased (figure 19).

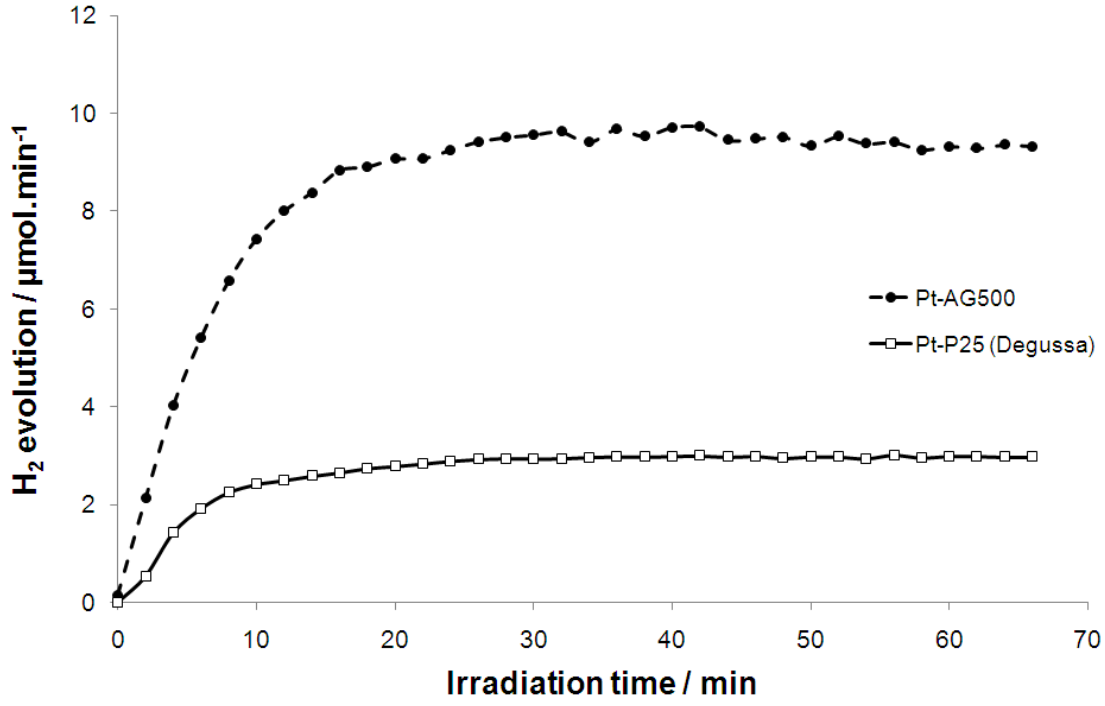

Fig. 19. H_2 evolution on TiO_2 Pt loaded samples : aerogel calcined at 500 °C and P25 - 150 W metal halide lamp, 0.9 l water + 0.1 l MeOH, 0.7 g samples, 0.3 wt% Pt/TiO_2, room temperature – Strasbourg, France.

This may be due to a synergetic effect of the two charge separation processes, ascribed to the peculiar aerogel morphology on one hand and to the co-catalyst on another hand. If we consider that the proton reduction on Pt particles is similar on both photocatalysts, the Pt particles seem to act as electron sinks

much more efficient on Pt-AG500 than on Pt-P25. The minor increase of activity observed on Pt-P25 may also be analysed with respect to the conclusion of Emilio et al. [45]. These authors claimed that the deposit of Pt particles on the surface of P25 has a negative effect on the phenol photodegradation whereas it is beneficial for pure anatase TiO_2, thus confirming the results of Sun et al. [41]. This conclusion is based on the assumption that the charge carrier separation process induced by Pt on pure anatase TiO_2 has no influence on P25 since the charge carrier separation process induced by the connection between anatase and rutile is already very efficient. Hence they claimed that negative effects of Pt, such as light absorption or the introduction of recombination sites, are prevalent to the beneficial ones. As a consequence, if the efficiency on anatase TiO_2 is increased after Pt deposit, that of P25 is decreased. Regarding our results, what is claimed for phenol photodegradation cannot strictly apply to hydrogen evolution. This may nevertheless be used to analyze the difference observed. After a closer look at the results presented by Emilio et al., it is noteworthy that the photoactivity of anatase supported platinum is similar to that of pure P25 (50 min are necessary to completely degrade phenol in both cases). This seems to indicate that the beneficial effect of Pt on anatase is comparable to that of mixing anatase and rutile, at least as far as phenol photodegradation is concerned (figure 20).

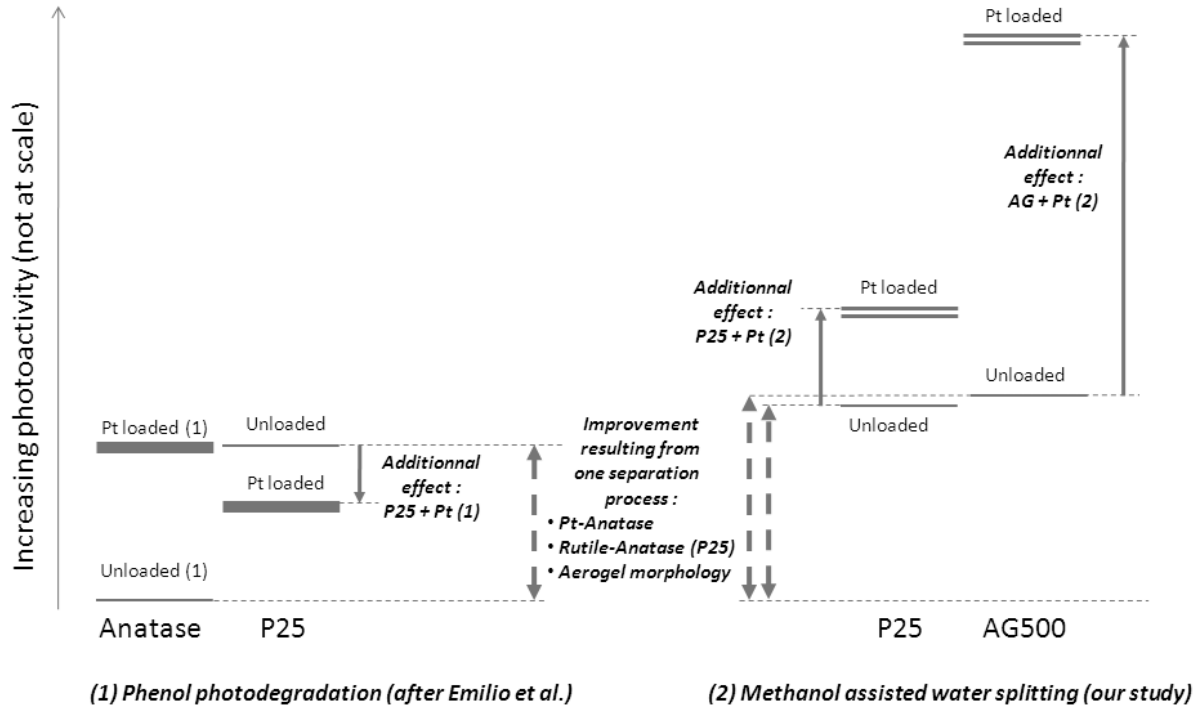

Fig. 20. Proposed diagram to compare and analyze the different photoactivities of our materials.

A similar observation can be made comparing our results on P25 and AG500. Provided that the specific morphology of AG500 may be responsible of its good photocatalytic activity, we have, here also, two different charge carrier separation processes leading to similar photoactivity. On the contrary to what Emilio et al. reported for phenol photodegradation, we have nevertheless observed an increase of activity, concerning H_2 evolution, for both catalysts supported Pt (figure 20). The water degradation kinetics might not be as a limiting step as phenol degradation kinetics, what could partially accounts for the additional activity induced by the Pt deposit. In both cases, two different charge carrier

separation processes are coupled : Pt deposit, plus the anatase-rutile interface for P25 or the aerogel morphology for AG500. The former interaction (Pt + anatase-rutile interface) is here again less efficient than the latter (Pt + aerogel morphology). This could partially account for a less impressive increase of photoactivity of Pt-P25 compare to that of Pt-AG500.

Pt-AG500, more than three times more active than Pt-P25 in the selected operating conditions, appears to be a good candidate for methanol assisted water splitting applications. The mesoporous texture of TiO_2 has recently been evidenced as a major feature to increase its photocatalytic activity [41], thus confirming the interest of aerogel materials in this area.

4. Conclusion

The different TiO_2 samples tested in this study have shown different photocatalytic behaviors, depending on both their composition and morphologies.

The nanoparticles we have tested revealed to be more active for H_2 evolution than the selected commercial anatase ones because of a higher specific surface area. Nevertheless, despite a higher specific surface area than P25, they were less active, stressing the point on the importance of a good charge carrier separation. The two other type of materials, namely nanotubes and aerogels, have been chosen because of the possible role of their specific morphology in the afore mentioned separation process. Our nanotubes exhibited promising performances but tend to decompose in nanoparticles. Made of TiO_2(B), they showed that, under UV irradiation, the use of 1D morphology combined with the mixture of two phases (TiO_2(B) and anatase as in NT400) could lead to a better activity than P25, while under "visible" irradiation the performances are only slightly below that of P25.

TiO_2 aerogels are very promising materials since they exhibit very good performances. Without Pt co-catalyst, they can reach the level activity of P25 for hydrogen evolution. The addition of 0.3 wt% Pt nanoparticles has even allowed to largely surpass that of Pt-P25, whose activity is already ten folds that of unsupported P25. We suppose that such a good behaviour may be ascribed to the beneficial interaction of two charge separation processes : one due to the use of Pt, already well illustrated in the literature, added to a process linked to the specific morphology of aerogels.

Aerogels photocatalysts will be more deeply investigated in our group, in order to clarify the origin of such good performances, that we think resides in their specific morphology, probably responsible of efficient charge carrier separation.

Acknowledgements

The authors wish to thank the CARNOT MINES Institute for financing this study and Pierre Ilbizian for SC CO_2 drying.

References

[1] Meng Ni, Michael K.H. Leung, Dennis Y.C Leung and K. Sumathy. A review and recent developments in photocatalytic water-splitting using TiO_2 for hydrogen production. Renewable and Sustainable Energy Reviews 2007; 11:401-425

[2] Akihido Kudo. Recent progress in the development of visible light-driven powdered photocatalyst for water splitting. International Journal of Hydrogen Energy 2007; 32:2673-2678

[3] Franck E. Osterloh. Inorganic materials as catalysts for photochemical splitting of water. Chemistry of Matterials. 2008; 20:35-54

[4] Akihido Kudo and Yugo Miseki. Heterogeneous photocatalyst materials for water splitting. Chemical Society Reviews 2009 ; 38(1):253-278

[5] J. Nowotny, T. Bak, M.K. Nowotny and L.R. Sheppard. Titanium dioxide for solar-hydrogen I. Functional properties. International Journal of Hydrogen Energy 2007; 32:2609-2629

[6] Akira Fujishima, Kenichi Honda. Electrochemical photolysis of water at a semiconductor electrode. Nature 1972; 238:37-38

[7] Yoshikazu Suzuki, Marie-Hélène Berger, Daniela D'Elia, Pierre Ilbizian, Christian Beauger, Arnaud Rigacci, Jean-François Hochepied, and Patrick Achard. Synthesis and microstructure of a novel TiO_2 aerogel-TiO_2 nanowire composite. Nano 2008; 3(4):1-7

[8] Tomoko Kasuga, Masayoshi Hiramatsu, Akihiko Hoson, toru Sekino, and Koichi Niihara. Formation of Titanium Oxide Nanotube. Langmuir 1998; 14:3160-3163

[9] Yoshikazu Suzuki, Benoit P. Pichon, Daniela D'Elia, Christian Beauger and Susumu Yoshikawa. Preparation and microstructure of titanate nanowire thin films by spray Layer-by-Layer assembly method . Journal of the Ceramic Society of Japan 2009 ; 117:381-394

[10] Antoine Bisson, Arnaud Rigacci, Didier Lecomte, Elisabeth Rodier and Patrick Achard. Drying of silica gels to obtain aerogels: Phenomenology and basic techniques. Drying Technology 2003; 21(4):593-628

[11] Souhir Boujday, Franck Wünsch, Patrick Portes, Jean-François. Bocquet, Christophe Colbeau-Justin. Photocatalytic and electronic properties of TiO_2 powders elaborated by sol-gel route and supercritical drying. Solar Energy Materials & Solar Cells 2004; 83:421-433

[12] A. S. Marfunin. Spectroscopy, luminescence and radiation centers in minerals. Springer-Verlag, Berlin 1979.

[13] J.I. Pankove, Optical Processes in semiconductors, Dover Publications, Inc, New York 1971; 34-44

[14] Thomas Beuvier, Mireille Richard-Plouet, and Luc Brohan. Accurate Methods for Quantifying the Relative Ratio of Anatase and TiO_2(B) Nanoparticles. J. Chem. Phys. C 2009; 113:13703-13706

[15] Olivier Rosseler, Muthukonda V. Shankar, Maithaa Karkmaz-Le Du, Loïc Schmidlin, Nicolas Keller and Valérie Keller. Solar light photocatalytic hydrogen production from water over Pt and Au/TiO_2(anatase/rutile) photocatalysts: Influence of noble metal and porogen promotion. Journal of Catalysis 2010 ;269(1) :179-190

[16] Jaturong Jitputti, Sorapong Pavasupree, Yoshikazu Suzuki, Susumu Yoshikawa. Synthesis and photocatalytic activity for water-splitting reaction of nanocrystalline mesoporous titania prepared by hydrothermal method. Journal of Solid State Chemistry 2007 ;180:1743–1749

[17] Muthupandian Ashokkumar. An overview on semiconductor particulate systems for photoproduction of hydrogen. International Journal of Hydrogen Energy 1998; 23:427–438.

[18] Thammanoon Sreethawong, Yoshikazu Suzuki, and Susumu Yoshikawa. Photocatalytic evolution of hydrogen over nanocrystalline mesoporous titania prepared by surfactant-assisted templating sol-gel process. Catalysis Communication 2005; 6(2):119–124.

[19] G. Schmid, M. Baumle, M. Greekens, I. Heim, C. Osemann, T. Sawatowski. Current and future applications of nanoclusters. Chem. Soc. Rev. 1999 28(3):179–185

[20] Radim Beranek and Horst Kisch.Tuning the optical and photoelectrochemical properties of surface modified TiO_2. Photochemical & Photobiological Science 2008; 7(1):40-48

[21] M. Koelsch, S. Cassaignon, J. F. Guillemoles, J. P. Jolivet. Comparison of optical and electrochemical properties of anatase and brookite TiO_2 synthesized by the sol–gel method . Thin Solid Films 2002; 403-404:312-319

[22] S. Monticone, R. Tufeu, A. V. Kanaev, E. Scolan and C. Sanchez. Quantum size effect in TiO_2 nanoparticles: does it exist?. Applied Surface Science 2000;162-163:565-570

[23] K. Madhusudan Reddy, Sunkara V. Manorama, A. Ramachandra Reddy. Bandgap studies on anatase titanium dioxide nanoparticles. Materials Chemistry and Physics 2002; 78:239–245

[24] R. Zallen, M.P. Moret. The optical absorption edge of brookite TiO_2. Solid State Communications 2006 137:154-157

[25] H. Tang, K. Prasad, R. Sanjinès, P.E. Schmid and F. Levy. Electrical and optical properties of TiO_2 anatase thin-films. Journal of Applied Physics 1994; 75(4):2042-2047

[26] Amy L. Linsebigler, Guangquan. Lu, John T. Yates. Photocatalysis on TiO_2 Surfaces: Principles, Mechanisms, and Selected Results. Chemical Reviews 1995; 95 (3): 735–758

[27] S.H. Tolbert, A.B. Herhold, C.S. Johnson and A.P. Alivisatos. Comparison of quantum confinement effects on the electronic absorption spectra of direct and indirect gap semiconductor nanocrystal. Physical Review Letters 1994; 73(24):3266-3269

[28] A.J. Nozik and R. Memming. Physical chemistry of semiconductor-liquid interfaces. Journal of Physical Chemistry 1996;100(31):13061-13078

[29] Jaturong Jitputti, Yoshikazu Suzuki, and Susuma Yoshikawa. Synthesis of TiO_2 nanowires and their photocatalytic activity for hydrogen evolution. Catalysis Communications 2008; 9(6):1265-1271

[30] T. Ohsaka, F. Izumi, Y. Fujiki. Raman spectrum of anatase TiO_2. Journal of Raman Spectroscopy 1978; 7(6):321

[31] Mouna Ben Yahia, Frederic Lemoigno, Thomas Beuvier, Jean-Sebastien Filhol, Mireille Richard-Plouet, Luc Brohan, Marie-Liesse Doublet. Updated references for the structural, electronic and vibrational properties of TiO_2(B) bulk using first-principles density functional theory calculations. Journal of Chemical Physics 2009; 130(20):204501

[32] Roger I. Bickley, Teresita Gonzalez-Carreno, John S. Lees, Leonardo Palmisano and Richard J. D. Tilley. A structural investigation of titanium dioxide photocatalysts. Journal of Solid State Chemistry 1991; 92:178

[33] Huang-Lin Kuo, Chih-Yin Kuo, Chun-Hsuan Liu, Jiunn-Hsing Chao, and Chiu-Hsun Lin. A highly active bi-crystalline photocatalyst consisting of TiO_2(B) nanotube and anatase particle for producing H_2 gas from neat ethanol. Catalysis Letters 2007; 113(1–2):7-12.

[34] Jaturong Jitputti, Sorapong Pavasupree, Yoshikazu Suzuki, Susumu Yoshikawa. Synthesis of TiO_2 nanotubes and its photocatalytic activity for H_2 evolution. Japanese Journal of Applied Physics 2008; 47(1):751-756

[35] Chiu-Hsun Lin, Jiunn-Hsing Chao, Chun-Hsuan Liu, Jui-Chun Chang and Feng-Chieh Wang. Effect of calcination temperature on the structure of a Pt/TiO_2 (B) nanofiber and its photo-catalytic activity in generating H_2. Langmuir 2008; 24(17):9907–9915.

[36] Geula Dagan and Micha Tomkiewicz. TiO_2 aerogels for photocatalytic decontamination of aquatic environments. The Journal of Physical Chemistry 1993; 97(49):12651-12655

[37] Vincenzo Augugliaro, Salvatore Coluccia, Vittorio Loddo, Leonardo Marchese, Gianmario Martra, Leonardo Palmisano and Mario Schiavello. Photocatalytic oxidation of gaseous toluene on anatase TiO_2 catalyst: mechanistic aspects and FT-IR investigation. Applied Catalysis B: Environmental 1999; 20(1):15–27

[38] L. Znaidi**,** R. Séraphimova**,** J. F. Bocquet**,** C. Colbeau-Justin and C. Pommier. A semi-continuous process for the synthesis of nanosize TiO_2 powders and their use as photocatalysts. Materials Ressearch Bulletin 2001; 36:811-825

[39] Thammanoon Sreethawong and Susumu Yoshikawa. Enhanced photocatalytic hydrogen evolution over Pt supported on mesoporous TiO_2 prepared by single-step sol–gel process with surfactant template. International Journal of Hydrogen Energy 2006; 31 :786 – 796

[40] Pierre Pichat, M.N. Mozzanega, Jean Didier and Jean-Marie Hermann. Pt content and temperature effects on the photocatalytic H2 production from aliphatic alcohols over Pt-TiO_2. New journal of chemistry 1982; 6(11):559-564

[41] Bo Sun, Alexandre V. Vorontsov, and Panagiotis G. Smirniotis. Role of Platinum Deposited on TiO_2 in Phenol Photocatalytic Oxidation. Langmuir 2003; 19:3151-3156

[42] S. Sakthivel, M.V. Shankar, M. Palanichamy, B. Arabindoo, D.W. Bahnemann and V. Murugesan. Enhancement of photocatalytic activity by metal deposition: characterisation and photonic efficiency of Pt, Au and Pd deposited on TiO_2 catalyst. Water Research 2004;38(13):3001-3008

[43] Mantana Moonsiri, Pramoch Rangsunvigit, Sumaeth Chavadej and Erdogan Gulari**.** Effects of Pt and Ag on the photocatalytic degradation of 4-chlorophenol and its by-products. Chemical Engineering Journal 2004; 97(2-3):241-248

[44] F.B. Li and X.Z. Li. The enhancement of photodegradation efficiency using Pt–TiO_2 catalyst. Chemosphere 2002; 48:1103-1111

[45] Carina A. Emilio, Marta I. Litter, Marinius Kunst, Michel Bouchard and Christophe Colbeau-Justin. Phenol photodegradation on platinized-TiO_2 photocatalysts related to charge carrier dynamics. Langmuir 2006; 22:3606-3613

[46] Singto Sakulkhaemaruethai and Thammanoon Sreethawong. Synthesis of mespporous-assembeld TiO2 nanocrystals by a modified urea-aided sol-gel process and their outstanding photocatalytic H2 production activity. International Journal of Hydrogen Energy 2011; 36:6553-6559